Melting scenario in metallic clusters

P. J. Hsu,[1] J. S. Luo,[1] S. K. Lai,[1,a)] J. F. Wax,[2] and J.-L. Bretonnet[2]
[1]*Complex Liquids Laboratory, Department of Physics, National Central University, Chungli 320, Taiwan*
[2]*Laboratoire de Physique des Milieux Denses, Université de Metz, 1. Bd FD Arago, 57078 Metz Cedex 3, France*

(Received 30 April 2008; accepted 7 October 2008; published online 18 November 2008)

The isothermal Brownian-type molecular dynamics simulation has been applied to study the melting behavior of bimetallic clusters. It was found that the specific heat and Lindermann-like parameter customarily used in bulk system to describe solid-liquid transition show incongruity in the predicted melting temperature T_{melt}. The underlying mechanisms that lead to the incompatibility of T_{melt} separately deduced from these two quantities were analyzed further. To gain insight into the melting behavior, we calculated in addition the velocity autocorrelation function and its Fourier transform, the power spectrum, and extracted from them the T_{melt}. It appears that the T_{melt} inferred from the latter quantities is closer to that deduced from the principal peak position of specific heat. Two bimetallic clusters, namely, Ag_1Cu_{13} and Au_1Cu_{13}, were selected for a thorough investigation. In the context of cluster morphology, we scrutinized the atomic distributions of Ag_1Cu_{13}, Au_1Cu_{13}, and Cu_{14} and effected a comparative study between a bimetallic cluster and a pure cluster so as to learn from comparison the differences in the thermal reaction of atoms, in particular, the impurity atom in the bimetallic cluster. On analyzing the dynamical data, we observed at a lower temperature ($T \ll T_{\mathrm{melt}}$) migrational relocation of atoms whose dynamics was superimposed at an intermediate temperature ($T < T_{\mathrm{melt}}$) by permutations between atoms, and at a higher temperature ($T \approx T_{\mathrm{melt}}$), liquidlike or even gaslike behavior. © *2008 American Institute of Physics*.
[DOI: 10.1063/1.3009194]

I. INTRODUCTION

Considerable efforts have been devoted to understand the melting phenomenon of bulk metallic systems. For a finite system such as the bimetallic cluster (BC), our grasp of its thermal response and the pertinent structural changes that result remains to be enriched, although attempts have already been made in recent years using simulation techniques[1–8] to uncover the melting mechanism of some of the BCs. In our preceding work,[8] we reported detailed simulation studies for small BCs Au_mCu_n ($m+n=13$ and 14) and pointed out the apparent incompatibility of the melting temperature T_{melt}, which is designated at the main peak of the specific heat C_V with that which is inferred from the relative root-mean-square (rms) bond length fluctuation parameter δ. The abrupt rise in δ at lower temperatures $T < T_{\mathrm{melt}}$ is due to the structural rearrangement or relocation of atoms in solid phase rather than the anticipated atomic diffusive motion observed ubiquitously in the bulk melting process. Since our preceding work was devoted to introducing an algorithm appropriate for studying the temperature dependence of BCs and in that work more thorough analysis was limited to only one BC, namely, Au_1Cu_{13}, it would appear that our understanding of melting mechanism in BCs needs still to be proliferated. In this work, we applied the same numerical recipe to study the thermal behavior of Ag_1Cu_{13}, another noble-metal-based BC. As we shall demonstrate below, the simulated results of Ag_1Cu_{13}, diagnosing in parallel with Au_1Cu_{13} and both comparing with respect to Cu_{14}, afforded a broader perception of the temporal response of atoms to temperature. We should stress that our emphasis in this work is on scrutinizing the finer details of melting transition that would disclose new features of the microscopic dynamics in BC. Besides the thermal and geometric properties, we extended simulation studies to include the dynamical property of the velocity autocorrelation function (VAF) and its Fourier transform, the power spectrum.

Our interest in these dynamical variables stems from the fact that their temperature dependences reveal the gas-, liquid-, and solidlike phases, and a comprehension of the transition from one phase to the other may help to elucidate further the melting phenomenon. For these two quantities, both nonmetallic and metallic clusters have been reported previously in the literature. One early attempt using the VAF to study solid-liquid transition in nonmetallic clusters is the isoenergetic simulation of Jellinek *et al.*[9] These authors applied the molecular dynamics (MD) simulation to calculate the VAF and its corresponding power spectrum for Ar_{13}. By examining the characteristics of VAFs and power spectra at different total energy values, they were able to isolate a solidlike phase and a liquidlike phase from a transition region of two coexisting phases; the latter is characterized by the cluster spending long time intervals in each phase and by it undergoing spontaneous transition from one form to the other in the course of its time development. In subsequent works, Beck *et al.*[10] and Beck and Berry[11] extended their simulation studies to larger clusters Ar_n ($n > 13$) and found that the coexistence of solid- and liquidlike forms in the

a)Electronic mail: sklai@coll.phy.ncu.edu.tw.

abovementioned transition region is not a smooth function of size n and is, in fact, not observed for clusters which can sample many minima (see Fig. 7 in Ref. 11). Another study which was devoted to capture the anomalous atmospheric absorption phenomena was communicated by Buffey *et al.*[12] Employing MD simulation, Buffey *et al.* obtained VAFs and their associated power spectra for a few large water clusters. They confirmed the hypothesis that the observed anomalous absorption of far infrared radiation by the atmosphere is due to large *liquidlike* water clusters. This same computational strategy was successfully used also by Zhang *et al.*[13] to predict for small metallic clusters Na_n $(n=2-8)$ at very low temperatures some of the experimental far infrared spectra. In several other investigations of metallic clusters which include for pure metallic cases, Mg_n,[14,15] Al_n,[16] Ni_n,[17–19] Ag_n,[19] and Au_n[19] and bimetallic cases Cu–Au[2] and Pd-based nanoalloys,[5] attention was directed mainly to uncover the underlying mechanisms of melting transition. Despite these variant interests, there is, however, one common feature in all of these calculations; the VAFs were calculated by averaging over all atoms building up the cluster, i.e., for a whole cluster (or for "shells"[5,16] of clusters). As we shall show below, one can gain much insight into the detailed microscopic dynamics of the VAF and its power spectrum if the latter are computed for each atom in the cluster, and for doing so, it enables one to correlate the dynamic features of individual atomic motions to changes in locations of the individual atoms with temperature.

To keep our discussion simple and analysis transparent, we first investigated the pure cluster Cu_{14} and presented the simulated results in considerable details. Then, with respect to it, we studied Ag_1Cu_{13} and determined similar thermal and dynamical quantities. We compared and contrasted the Ag_1Cu_{13}, Au_1Cu_{13}, and Cu_{14} and looked into the role played by the "impurity" atom in BC. This exploration is interesting for, structurally, the atomic distribution of Ag_1Cu_{13} and of Au_1Cu_{13} are totally different: The former has silver atom floating outside an icosahedral surface, whereas the latter has gold atom residing at the central position of the icosahedron. It would thus be interesting to contrast how, on the one hand, the pure cluster Cu_{14} and, on the other hand, the impurity atom in BC affect the thermal development of the whole cluster.

The present paper is organized as follows. In Sec. II, we give a brief description of the algorithm of the isothermal Brownian-type MD simulation developed for BC. Equations for the many-body Gupta potential and for the thermal, geometrical, and dynamical quantities will be summarized in this section. The simulated data for Cu_{14} will first be analyzed quantitatively in Sec. III, and with respect to it, we next present simulation results of Ag_1Cu_{13} and finally Au_1Cu_{13}. In Sec. IV, we give a conclusion.

II. METHODOLOGY: SIMULATION AND THEORY

A. Simulation algorithm: Isothermal Brownian-type molecular dynamics

In this section, we document the numerical tools and give the essential theoretical formulas required in the present simulations.

1. Equations of motion

To begin with, we describe the isothermal Brownian-type MD method and the generalization of it to the BC. We employ the modified cubic coupling scheme[8] which is readily generalized to an alloy cluster $A_{n_a}B_{n_b}$, where n_a (n_b) is the number of atoms of a type (b type). Explicitly, the equations of motion (for the x component) can be written as

$$\dot{x}_{i(a)} = \frac{p_{i(a),x}}{m_a}, \tag{1}$$

$$\dot{p}_{i(a),x} = -\frac{\partial E_n}{\partial x_{i(a)}} - \frac{\alpha_a e_{0,a}}{nL_0}\mu_{a,x}^3 \frac{p_{i(a),x}}{p_{0,a}} - \frac{\beta_a e_{0,a}}{nL_0}\nu_{a,x}\left(\frac{p_{i(a),x}^2}{p_{0,a}^2} - d_0\right) - \frac{\varkappa_a e_{0,a}}{nL_0}\eta_{a,x}\frac{p_{i(a),x}^3}{p_{0,a}^3}, \tag{2}$$

in which the subscript $i(a)$ refers to ith atom of a type, and the x-component pseudofriction coefficients $\mu_{a,x}$, $\nu_{a,x}$, and $\eta_{a,x}$ of a-type atoms, which are introduced to simulate the heat bath degrees of freedom,[20,21] are to be determined from

$$\dot{\mu}_{a,x} = \frac{\alpha_a T}{p_{0,a}L_0}\left(\frac{\Sigma_{i=1}^{n_a} p_{i(a),x}^2}{nm_a T} + \frac{\Sigma_{i=1}^{n_b} p_{i(b),x}^2}{nm_b T} - 1\right), \tag{3}$$

$$\dot{\nu}_{a,x} = \frac{\beta_a T}{p_{0,a}L_0}\left(\frac{\Sigma_{i=1}^{n_a} p_{i(a),x}^3}{nm_a T p_{0,a}} + \frac{\Sigma_{i=1}^{n_b} p_{i(b),x}^3}{nm_b T p_{0,b}} - d_0\frac{\Sigma_{i=1}^{n_a} p_{i(a),x} p_{0,a}}{nm_a T} - d_0\frac{\Sigma_{i=1}^{n_b} p_{i(b),x} p_{0,b}}{nm_b T} - \frac{2\Sigma_{i=1}^{n_a} p_{i(a),x}}{np_{0,a}} - \frac{2\Sigma_{i=1}^{n_b} p_{i(b),x}}{np_{0,b}}\right) \tag{4}$$

$$\dot{\eta}_{a,x} = \frac{\varkappa_a T}{p_{0,a}L_0}\left(\frac{\Sigma_{i=1}^{n_a} p_{i(a),x}^4}{nm_a T p_{0,a}^2} + \frac{\Sigma_{i=1}^{n_b} p_{i(b),x}^4}{nm_b T p_{0,b}^2} - \frac{3\Sigma_{i=1}^{n_a} p_{i(a),x}^2}{np_{0,a}^2} - \frac{3\Sigma_{i=1}^{n_b} p_{i(b),x}^2}{np_{0,b}^2}\right). \tag{5}$$

In Eqs. (1)–(5), T is the temperature in Kelvin, and $x_{i(a)}$ and $p_{i(a),x}$ are the x-component position coordinate and momentum, respectively. For b-type atoms, we simply replace the subscript a by b in Eqs. (1)–(5). The same set of equations hold for the y and z components. In Eq. (2), E_n is the potential energy to be given by Eq. (6) below. The quantities m_a and $p_{0,a}=\sqrt{2m_a T}$ are the atomic mass and average thermal momentum at temperature T of an a-type atom, respectively, and d_0 is a dimensionless constant with a value of the order of 1. L_0 is also a constant with the dimension of length and numerically is of the order of 1 Å. The quantity $e_{0,a}$, which first appears in the time dependent canonical distribution,[22] is an energy constant whose value can be estimated as $e_{0,a} \sim m_a L_0^2 \omega_D^2/(4\pi^2)$. The magnitude of $e_{0,a}$ is thus of the order corresponding to a free cluster exhibiting a Debye frequency ω_D. Lastly, $\alpha_a \sim \beta_a \sim \varkappa_a \sim [m_a L_0^2/(nTt_0^2)]^{1/2}$, in which $t_0 = 2\pi/\omega_D$ is the smallest characteristic time scale of the system, are cluster independent constants.

Considering the kind and the size of BCs to be studied in this work, we have experimented different ranges of values for the aforementioned constant parameters and finally arrived at an optimized set of values. They are $L_0=1$ Å, d_0

$=1$, and $\omega_D=60\times10^{12}$ s^{-1}. Although other choice of these constants is possible, the quality of the simulation results would not be affected providing that the simulations are performed at long enough times. In this work, the equations of motion were integrated numerically using the Hamming predictor-corrector method of fourth order. With the chosen set of parameters, this integration algorithm allows a larger time step (up to $\Delta t=10^{-14}$ s) to be used. At each T, the simulation run was carried out for at least 0.2×10^8 steps. Much longer simulation time of $(6-10)\times10^7$ steps was performed for clusters in the temperature region showing the premelting-like feature and in the meltinglike transition region. The total elapsed time t_{tot} for each MD run was therefore $t_{\text{tot}}=10^{-7}$ s. In actual simulations, we found that $\Delta t=1-5\times10^{-15}$ s is generally sufficient for the quantities studied here. There were, however, exceptional cases where larger fluctuations were encountered. When any of the latter happens, using $\Delta t\leqslant0.5-10^{-15}$ s in the MD simulation will normally improve the simulation results. The time step $\Delta t=10^{-15}$ s works well also in the lower temperature region ($T<100$ K). As regards the temperature increment, we run the MD simulation at an interval of 10 K in all regions including the premelting and meltinglike regions.

2. Many-body Gupta potential

To account for the many-body interactions between metallic atoms, we employ the widely used n-body Gupta potential.[23,24] This empirical potential reads

$$E_n=\sum_{i=1}^{n}\left\{\sum_{j=1(j\neq i)}^{n}A_{ij}\exp\left(-p_{ij}\left(\frac{r_{ij}}{r_{ij}^{(0)}}-1\right)\right)-\left[\sum_{j=1(j\neq i)}^{n}\xi_{ij}^2\exp\left(-2q_{ij}\left(\frac{r_{ij}}{r_{ij}^{(0)}}-1\right)\right)\right]^{1/2}\right\},\tag{6}$$

where A_{ij}, ξ_{ij}, p_{ij}, q_{ij}, and $r_{ij}^{(0)}$ are parameters fitted to bulk measured data of lattice constant, cohesive energy, and elastic constants for the face-centered-cubic crystalline structure at 0 K. There are three sets of parameters of which two sets are homonuclear ($i=j$), one for Cu–Cu and the other for Au–Au, and the third set is heteronuclear ($i\neq j$) for Cu–Au. The former sets are adjusted to bulk data taken from the pure Cu and Au metals and are assumed the same in the BC; the latter set is determined by fitting to the crystalline structure of an intermetallic compound. In this work, we use the parametric values (Table I) of Cleri and Rosato[23] and Mottet *et al.*[25] We refer the interested readers to their works for further details.

TABLE I. Gupta-type potential parameters for the bimetallic clusters Cu–Ag and Cu–Au taken from Mottet *et al.* (Ref. 25) and Cleri and Rosato (Ref. 23), respectively. $r_{ij}^{(0)}$ is scaled by the Bohr radius.

ij	A_{ij} (eV)	ξ_{ij} (eV)	p_{ij}	q_{ij}	$r_{ij}^{(0)}$
		CuAg			
Cu–Cu	0.089 4	1.2799	10.55	2.43	2.56
Cu–Ag	0.097 7	1.2275	10.70	2.805	2.725
Ag–Ag	0.103 10	1.1895	10.85	3.180	2.89
		CuAu			
Cu–Cu	0.085 5	1.2240	10.960	2.2780	2.556
Cu–Au	0.153 9	1.5605	11.050	3.0475	2.556
Au–Au	0.206 1	1.7900	10.229	4.0360	2.884

B. Thermal and geometric properties

1. Specific heat and Lindemann-like parameter

For the thermal property, we calculated the specific heat C_V. This quantity is straightforwardly computed since the configuration energies were readily recorded by the above equations. Explicitly,

$$C_V(T)=\frac{\langle E_{\text{total}}^2\rangle_t-\langle E_{\text{total}}\rangle_t^2}{k_BT^2},\tag{7}$$

where $E_{\text{total}}=(\Sigma_{i(a)}p_{i(a)}^2/(2m_a)+\Sigma_{i(b)}p_{i(b)}^2/(2m_b))+E_n$. A cluster at temperature T is heated up from its lowest energy configuration until it transforms into a liquidlike cluster. We have performed for each BC rather long simulation time (1×10^{-7} s) so that the calculated C_V vs T curves develop as smooth as possible. Any larger fluctuation that still remains would point to the need to improve the coupling scheme.

For the geometric property, we calculated the relative rms bond length fluctuation constant δ. This quantity which dictates the geometric property is defined by

$$\delta=\frac{1}{n(n-1)}\sum_{i=1}^{n}\sum_{j\neq i}^{n}\frac{\sqrt{\langle r_{ij}(t)^2\rangle_t-\langle r_{ij}(t)\rangle_t^2}}{\langle r_{ij}(t)\rangle_t},\tag{8}$$

where n is the total number of atoms in cluster. Since the geometric information buried in δ is analogous to that encountered in a bulk system, δ may be called the Lindemann-like parameter. When T is below the meltinglike transition temperature, the cluster behaves very much like a typical solid; the atoms are characterized by vibrational motion about their equilibrium sites, and δ assumes a small and nearly constant value. On the contrary, a drastic change of δ in some temperature range would be expected (as seen in bulk systems) to signal some kind of the structural or phasic transformation. For the purpose of quantitative analysis of the melting behavior of BCs and the fact that BCs have the unique structural property of manifesting isomerization transitions involving permutational (in addition to topological) isomers, it is instructive to record two additional sets of data.

The first set aims at revealing the temporal evolution of a cluster when it is maintained at given T. To this end, we rewrite Eq. (8) in an equivalent form

$$\delta=\frac{1}{n(n-1)}\sum_{i=1}^{n}\sum_{j\neq i}^{n}\frac{\sqrt{\langle(r_{ij}(t)-\langle r_{ij}(t)\rangle_t)^2\rangle_t}}{\langle r_{ij}(t)\rangle_t},\tag{9}$$

so that δ can be analyzed by following the trajectory of the instantaneous relative bond length $r_{ij}(t)$. At given temperature, the temporal development of r_{ij} discloses the microscopic dynamics of ij atoms (within the n-atom cluster) of the same and different kinds. Strategically, $r_{ij}(t)$ can be obtained as follows. For a cluster regulated at given T, we

effected isothermal Brownian MD simulations at $\Delta t = 10^{-15}$ s and run for a total simulation time of 100 ns. We recorded $r_{ij}(t)$ in two ways. For the pure cluster Cu_{14}, $r_{ij}(t)$ was recorded at every 100 Δt for a total number of 2×10^5, and for BC, we recorded $r_{ij}(t)$ at every 10^4 Δt, which is, in fact, an average value obtained by $[r_{ij}(t_1)+\cdots r_{ij}(t_{10})]/10$, where $r_{ij}(t_i)$ was calculated at every $t_i=10^3$ Δt. In this case, we collected $r_{ij}(t)$ for a total number of 10^4.

The second set directs to constructing the temperature dependent energy histograms and the use of them to supplement our interpretation of $r_{ij}(t)$. To accomplish this, we run the simulation for 100 ns, after an equilibrium time of 25 ns. At any fixed T, we collected configurations from every 50 Δt increment. A total number of 1.5×10^6 configurations was stored. Starting with these atomic geometries which were treated as initial configurations, we applied the L-BFGS minimization algorithm[26] to locate their corresponding local energy minima. The local energy minima of all these configurations were then recorded. Since the procedure was effected at each prescribed T, the distribution of the local energy minima yields the desired temperature dependent energy histograms.

C. Dynamical property

1. Velocity autocorrelation function and power spectrum

When atoms in a bulk solid are heated up, they respond in the form of increasing oscillatory amplitude at their respective solidlike locations. At a temperature, say, near melting, the vibrational behavior of atoms strays far from their solidlike sites and a switch over to liquidlike diffusive motion happens. Since the cluster is a finite-sized system, the displacement of atoms has to be bounded (which connotes the diffusion constant equal to zero) and cannot therefore continue to grow with time.[27] Consequently, there remains an ambiguity in the mean square displacement of atoms in a cluster to reach the linear asymptotic evolution with time which is the characteristic behavior of the diffusion in bulk liquids. Therefore, a more useful quantity for observing such a dynamical behavior may be the VAF, which is defined by

$$C(t) = \frac{\sum_{i=1}^{n}\sum_{j=1}^{M}\vec{\mathbf{v}}_i(t_{0j})\cdot\vec{\mathbf{v}}_i(t_{0j}+t)}{\sum_{i=1}^{n}\sum_{j=1}^{M}\vec{\mathbf{v}}_i(t_{0j})\cdot\vec{\mathbf{v}}_i(t_{0j})}. \tag{10}$$

Here, n is the total number of atoms and M is the number of time origins t_{0j} taken along a trajectory. Keeping track on $C(t)$, one would be able to see it changing from an oscillatory structure at low temperatures to a structure characterized by one minimum followed by a weak oscillatory decaying tail at high temperatures. This is the dynamical picture of a bulk metallic system varying with temperatures.[28] For a cluster which is a finite system, the situation is somewhat complicated. At low temperatures before melting ($T \ll T_{\mathrm{melt}}$), there already occur different kinds of atomic movement. Consider the 14-atom cluster. It comprises an icosahedron and a floating atom residing outside. Due to its location on the outer surface, the floating atom interacts weakly with its inner side neighboring atoms and is thus relatively free to wander about exhibiting, for example, a kind of migrational relocation from one (symmetrical) site to another. Since the amount of energy required for such a relocation is generally small, the floating atom may just perform the migrational relocation at a lower temperature; in other words, there will be no accompanied permutation between it and any atom of the icosahedron. At slightly higher temperatures, the atomic migrational relocation will gradually be superimposed by occasional permutations between the floating and surface atoms. The migrational motion will, however, decline at higher temperatures. A means to understand the underlying dynamics is to dissect the temperature dependences of the characteristic of $C(t)$. For a quantitative and deeper insight into the microscopic dynamics, it would be instructive to trail instead the individual particle since atoms in a cluster are distributed with varying neighbors. Accordingly, we consider

$$C^{(i)}(t) = \frac{\sum_{j=1}^{M}\vec{\mathbf{v}}_i(t_{0j})\cdot\vec{\mathbf{v}}_i(t_{0j}+t)}{\sum_{j=1}^{M}\vec{\mathbf{v}}_i(t_{0j})\cdot\vec{\mathbf{v}}_i(t_{0j})}, \tag{11}$$

which is the normalized VAF for the ith atom. Here, we make two relevant remarks. The first remark concerns Eq. (11). That $C^{(i)}(t)$ is preferred to $C(t)$ is based on the observation that the average over particles in $C(t)$, which is usually done in studies of bulk systems, is introduced as a way to improve the statistical accuracy, and implicitly, it presupposes the motion of all particles describing the same features. Since the small-time limit of VAF is inversely proportional to the mass of the atom,[29] it is more convenient to consider a normalized function in the case of BCs. The second remark involves the velocities of atoms which need to be corrected for the translational as well as the rotational motion of the whole cluster. Failing to do that will result in a nonzero value of the long time limit of $C^{(i)}(t)$. Having introduced $C^{(i)}(t)$, another useful quantity is the power spectrum

$$\Omega^{(i)}(\omega) = 2\int_0^\infty C^{(i)}(t)\cos(\omega t)dt. \tag{12}$$

This function projects out the underlying frequencies of the individual atomic processes. Physically, $\Omega^{(i)}$ corresponds to the infrared spectra of the system, and it reveals the vibrational behavior on an atomic scale. In bulk materials, this low frequency limit pertains to the diffusion coefficient which is nonzero for atoms in a liquid phase. Although the latter trait is not valid in finite-sized clusters where the self-diffusion coefficient is yet to be clarified,[9,27] this feature of the power spectrum nevertheless appears to be preserved as we will see shortly in following sections that report the calculated results. The characteristic changes of $C^{(i)}(t)$ and $\Omega^{(i)}(\omega)$ with temperature will be illustrated below for BCs as well as for Cu_{14}.

III. NUMERICAL RESULTS AND DISCUSSION

The cluster Cu_{14} will first be thoroughly described and analyzed. Then, we compared Cu_{14} with Ag_1Cu_{13} and Au_1Cu_{13} to examine the effects of the influence of impurities atoms Ag and Au in their respective BC. The comparison is interesting for the former has the Ag atom located at the floating position with respect to the icosahedron and the latter has the Au atom occupied the central site of icosahedron.

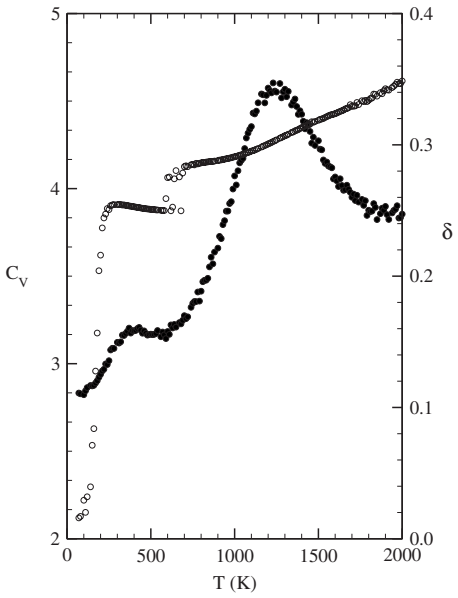

FIG. 1. The constant volume specific heat C_V and relative rms bond length fluctuation constant δ for Cu_{14}. The simulation runs were carried out at $\Delta t = 5 \times 10^{-15}$ s.

A. Pure cluster Cu_{14}

1. Specific heat and relative rms bond length fluctuation parameter

The lowest energy structure of Cu_{14} may be viewed in two ways. With respect to the 13-atom icosahedron, we may consider the 14th atom either "floats" at a site above three triangular shape atoms of which one is the apex atom and two others pertained to a nearby pentagonal ring or floats between two pentagonal rings but residing closer to one ring than the other. The C_V and δ of this cluster as a function of temperature have been reported previously;[8] they are reproduced in Fig. 1 for the convenience of discussion below. Figure 2(a) displays the lowest energy geometry; this structure persists up to $T=110$ K. At a slightly increased temperature $T=120$ K, we detected the first excited state [Fig. 2(b)], although its occurrence is comparatively low but is discernible (Fig. 3), however. The second excited state was found at a higher temperature $T \simeq 690$ K [Figs. 2(c)]. Notice that the energy of this excited state is degenerate. The third and higher excited states emerge at much higher temperatures ($T \gtrsim 800$ K). The normalized energy histograms given in Fig. 3 dictate the probability of occurrence of these energy states.

We begin our analysis with the specific heat C_V. Referring to Fig. 1, there are two well-resolved peaks, one at $T \approx 430$ K and the other at $T \approx 1230$ K. The first peak, as implied in our preceding work,[8] may be ascribed to atoms effecting surface reconstruction or the so-called premelting phenomenon, whereas the second maximum may be translated to be the solid-liquid-like melting with atoms in cluster performing diffusivelike motion as in a bulk system. To give concrete support to our interpretation, we examined the two-step changes of δ. The first step which shows an abrupt rise in δ (from 0.020 to 0.24) occurs in the temperature range $110 \lesssim T \lesssim 210$ K, and the second step where δ climbs up less severely (from 0.25 to 0.27) spans a temperature interval of

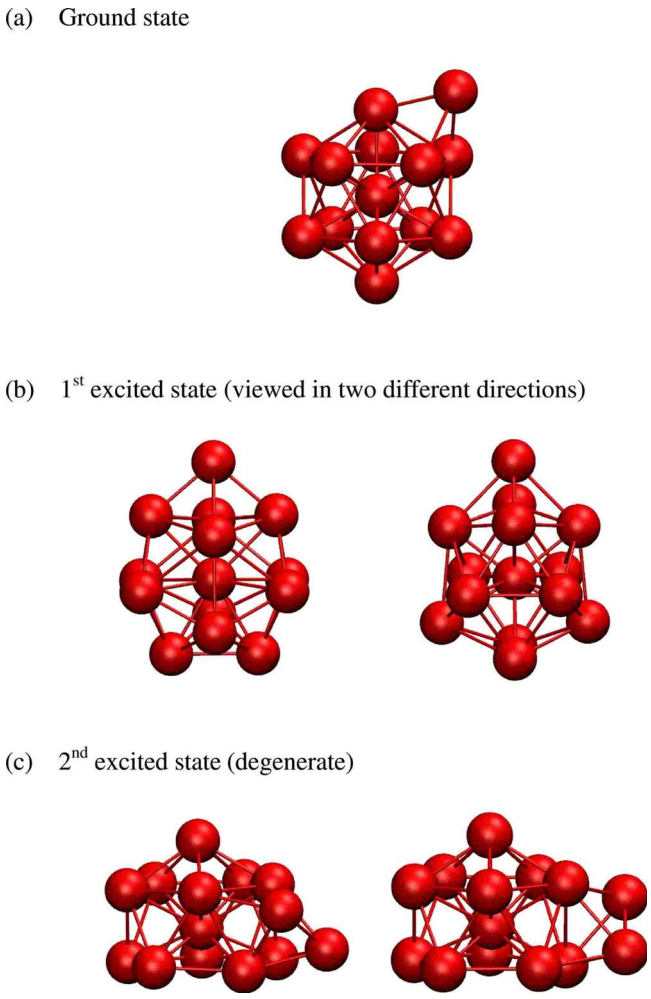

FIG. 2. (Color online) Structures of the lowest energy and excited states for pure metallic cluster Cu_{14}.

approximately 50 K. These variations in δ can be construed as follows. For the first step, the drastic rise in δ may be traced to the motion of the floating atom. This is evident in Fig. 3 where the cluster is certain to take on the lowest energy state for $T \lesssim 110$ K; as a result, δ increases but little. The first excited state comes in only at $T \simeq 120$ K. In our simulation, this first excited (as well as the lowest energy) state persists for the range of temperature $120 \lesssim T < 690$ K. The sudden increase in δ for $110 \lesssim T \lesssim 210$ K is thus likely to be a manifestation of the lively role of the floating atom whose location in the cluster accounts for the structural difference between the lowest energy [Fig. 2(a)] and first excited [Fig. 2(b)] states. To gain deeper insight into the geometric characteristic of δ and hence an understanding of the possible microscopic mechanism of melting, let us take a closer look at the temporal response of the atoms. To this end, we give in Table II the numerical values of r_{ij}, which are approximate distances estimated among the floating, surface, and central atoms hereafter designated as f, s_i, and c. These numerical data are useful guide for tracking the pair of ij atoms that had undergone permutation or, for the case of f atom at a lower temperature, had effected a migrational relocation [consult Figs. 4(a)–4(c) for the meaning of f-s_i, c-f, etc.]. We proceed now to analyze the time development of the cluster.

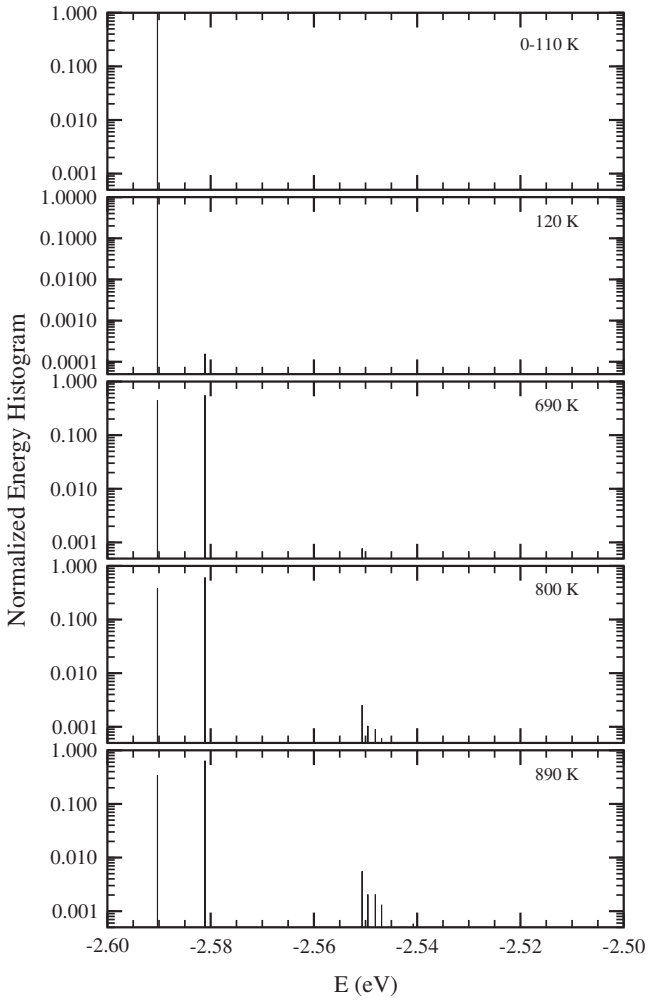

FIG. 3. Energy histograms of Cu_{14} constructed from isothermal Brownian-type MD simulations (see text) at temperatures $T=0-110$, 120, 690, 800, and 890 K.

Recall, first of all, that the first excited state appears only at $T \simeq 120$ K [Figs. 2(b) and 3]. As the cluster was heated up to a temperature at, say, $T=130$ K, we found the f atom wandering around the icosahedron resulting in the rise and fall of r_{ij} [green and blue lines in Fig. 5(b) and green line in Fig. 5(c)], but these up-and-down steps are *not* due to the permutational isomer transition between atoms of the kind f-s_i shown in Fig. 4(a). Instead, they are simply the movement of the f atom to a location above three-atom sites [Fig. 2(a)]. For although there is also the possibility of the f-atom

TABLE II. Approximate r_{ij} distance between floating (f), surface (s), and central (c) atoms. The up-and-down steps observed in r_{ij} indicate the pair of ij atoms that have got involved in permutation. The numerical values are used as a guide to tell the pair of ij atoms that have led to the rise and fall of r_{ij}. Notation used: Subscript i in s_i of columns two, three, four, and six refers to the surface atoms in the three-atom layer given in Fig. 4(a); subscript T or B in the third column refers to a surface atom as indicated in Fig. 4(b); subscript P_i in s_{p_i} of columns four and six refers to the surface atoms in the layer shown in Fig. 4(b).

ij atom	f-s_4	f-s_3, s_T-s_B	f-s_2, s_T-s_{p_2}, or s_B-s_{p_1}	c-f	c-s_i, s_T-s_{p_1} or s_B-s_{p_2}, f-s_1
r_{ij}	~6	~5	~4.1	3.8	~2.5

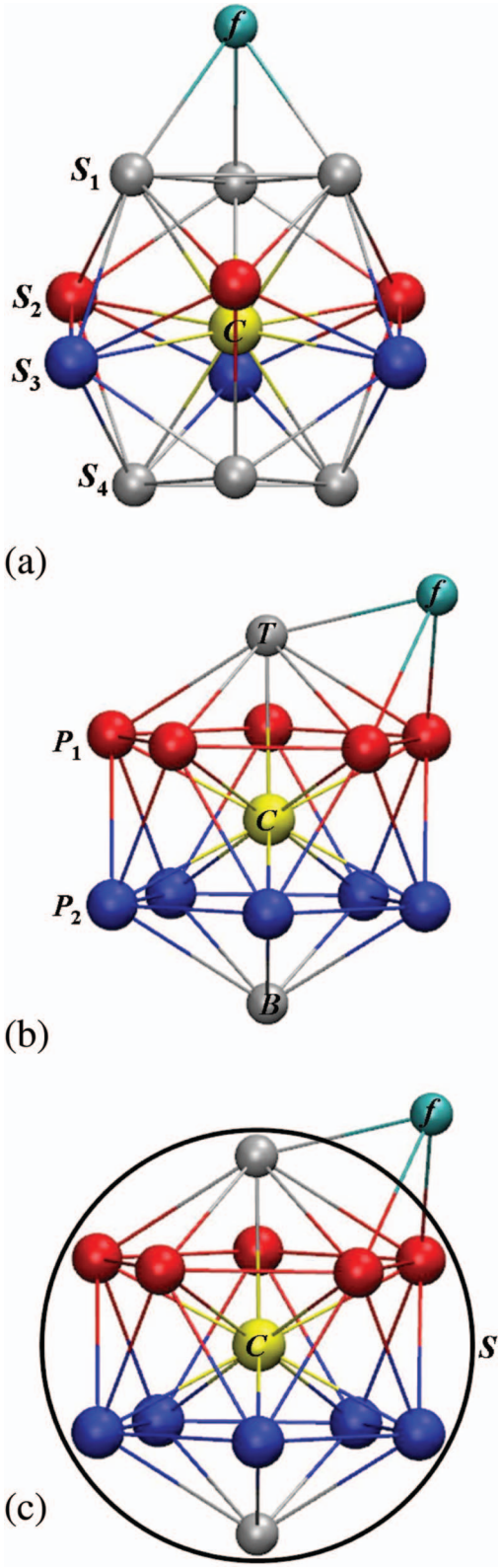

FIG. 4. (Color) Schematic diagrams for a 14-atom bimetallic cluster used to describe the permutational isomer transitions. (a) The cluster is turned so that the floating atom (f) is on top, and the surface atoms are split into four three-atom layers (s_1, s_2, s_3, and s_4) distinguished for clarity by different colors and the central atom is labeled c. (b) Another view of the 14-atom bimetallic cluster with the floating atom (f) residing outside an icosahedron, the top and bottom atoms are denoted by T and B, two pentagonal rings are designated by P_1 and P_2, and the central atom is labeled c. (c) The 14-atom bimetallic cluster is described by the floating (f), central (c), and surface (s) atoms. The s atoms enclosed within the circle are less of the c atom.

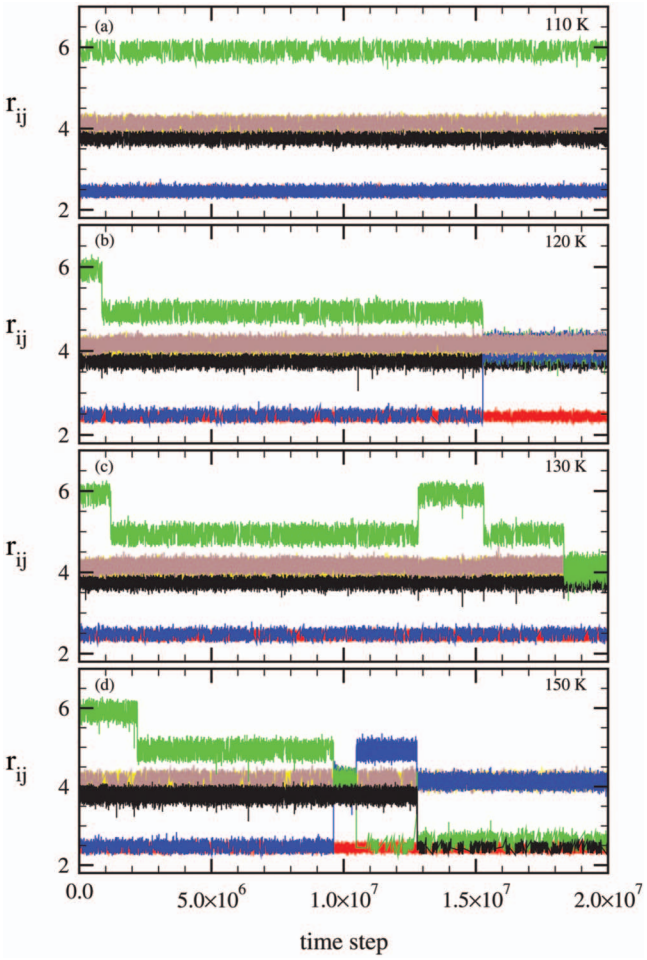

FIG. 5. (Color) Instantaneous relative bond length $r_{ij}(t)$ (see text) vs time step (in units of 5×10^{-15} s) obtained from isothermal Brownian-type MD simulations for Cu_{14} calculated at $T=110$, 120, 130, and 150 K. The rows (a)–(d) describe $r_{ij}(t)$, with i and j chosen from six sets of two atoms. Refer to Fig. 4(a) for the labeling of f, c, and s_i atoms. Notations used: Green, f-s_k; blue, f-s_l; yellow, s_i-s_j; brown, s_m-s_n; black, c-f; red, c-s_k. In (a), there are six pairs of ij atom (numerical values given in Table II should be consulted for identifying the possible permutation of the ij atom). Also, the yellow and red lines are behind the brown and blue lines, respectively. In (b) and (c), the up-and-down green and blue r_{ij} dictate the migrational relocation of the floating atom. No permutation between atoms are observed. In (c), more frequent migrational relocation for f-s_k (green). In (d), there are now migrational relocation as well as permutation between floating and surface atoms (green and blue) because the r_{ij} of c-f (black) fluctuates stepwise at the time step $\sim1.3\times10^7\ \Delta t$ and can be traced to the exchange of floating and surface atoms.

migrating to four-atom sites [Fig. 2(b)], we should remark that, at this temperature, the time spent in this first excited state is extremely low (Fig. 3). Coming back to Fig. 5(c), the black colored r_{ij}, which describes the c-f, should be read jointly with other r_{ij}'s in the same figure. The fact that c-f indicates *no* sign of up-and-down steps gives unambiguous evidence to our interpretation of the f atom performing purely relocation. Permutational activities between atoms of the kind f-s_i [Fig. 4(a)] were, however, observed only at an elevated temperature, even though slightly higher. As an illustration, we presented in Fig. 5(d) the sets of r_{ij} simulated at $T=150$ K. In contrast to r_{ij} at $T=120$ and 130 K depicted in Figs. 5(b) and 5(c), respectively, we noticed in Fig. 5(d) that not only the up-and-down r_{ij}'s come from the f atom effecting pure relocation (green, blue, and black lines for time step before $1.3\times10^7\ \Delta t$), but now also from the f atom performing the f-s_l (hence c-f) permutation (black line) at the specific time step $\sim1.3\times10^7\ \Delta t$. We did not observe any climbing or declining step in the r_{ij} between the central and surface atoms (red). Presumably, the latter s_l in f-s_l is not the same surface atom that participates in permutation (hence, we labeled s_k in c-s_k). Neither did we notice in Fig. 5(d) the r_{ij} among surface atoms fluctuates stepwise and, for the same reason, we wrote s_i-s_j and s_m-s_n. As the temperature increases further to 260 K (Fig. 6), more frequent permutations between the floating and surface atoms (left column) and also among surface atoms (middle column) occur, but the rising-and-falling steps seen for c-s_k and c-f (right column) are due to the migrational motion of f atom or the f-s_l permutations, rather than the exchange movement between the c atom and floating *or* surface atom. Since the cluster at this temperature is still in a solidlike phase, it is instructive, in a more detailed analysis, to consult Table II and the schematic diagrams shown in Figs. 4(a) and 4(b) for c-f, c-s_k, f-s_l, and perhaps s_T-s_B for recognizing the microscopic permutations. The situation becomes much more complex at, say, $T=500$ K for now the r_{ij} manifests rather high frequency of permutations among floating and surface atoms (not shown). It should be noted that, even at this temperature, the central atom still remains intact at the central position, and with respect to it, only the f atom migrates in an extremely high frequency to reside at a new site and exchange of sites occupied by the floating and surface atoms is incessant.

We turn next to the second rise of δ which falls in the temperature range spreading approximately from 570 to 620 K. Now, the central atom actively participates in permutations of the kind c-f or c-s_k. As a result, the lifetime for any atom that had been permuted into the central position and stayed there decreases with temperature and this scenario occurs at temperatures $T\gtrsim600$ K [cf. right columns of Figs. 7(a) and 7(b)]. It appears that at $T=800$ K, permutations among central, surface, and floating atoms culminate since up-and-down steps are indistinguishably close.

2. Velocity autocorrelation function and power spectrum

The temporal characteristics of r_{ij} have provided us with a platform to view the dynamics of atoms in a cluster. Scrutinizing $r_{ij}(t)$, we now understand that the floating, surface, and central atoms are responding differently to temperature depending on how the atom under consideration couples to its neighbors. To have a panoramic view of the melting phenomenon of a cluster, we turn to another useful dynamical quantity, namely, the VAF for the floating ($C^{(f)}$), surface ($C^{(s)}$), and central ($C^{(c)}$) atoms. In Figs. 8(a)–8(c), we display $C^{(i)}$ and also their corresponding $\Omega^{(i)}$ placed on the same rows next to them. The following features can be gleaned.

(a) For temperatures $T\leqslant300$ K, all of 14 $C^{(i)}$ exhibit pronounced oscillations that last for a long correlation time of 2.5 ps. This collective oscillatory behavior is reminiscent of the infrared molecular vibration. The

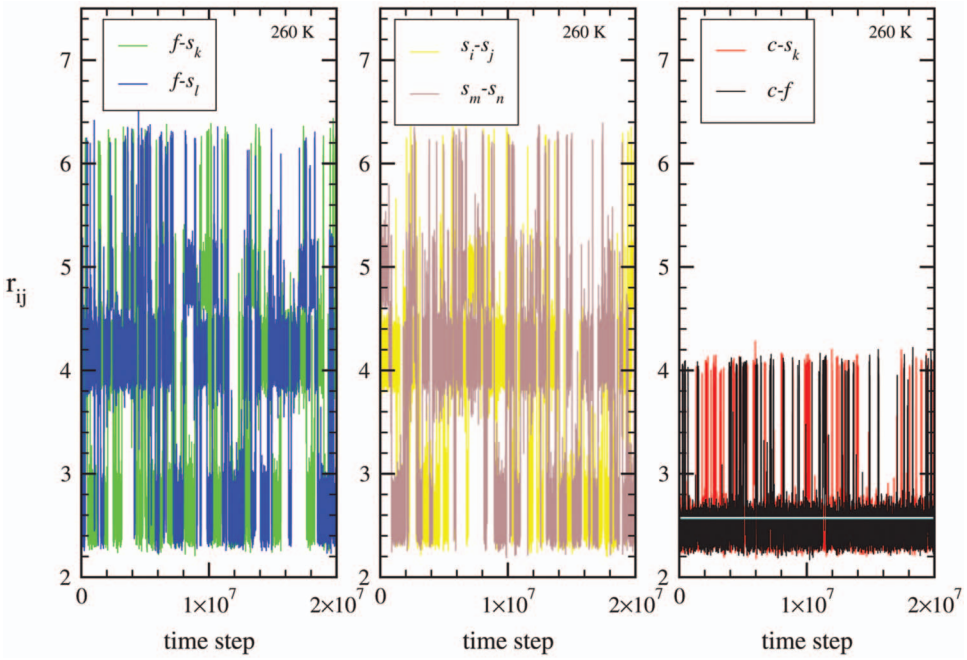

FIG. 6. (Color) Instantaneous relative bond length $r_{ij}(t)$ vs time step (in units of 5×10^{-15} s) obtained from isothermal Brownian-type MD simulations for Cu_{14} calculated at $T=260$ K. Same notations as in Fig. 5. The permutational isomer transitions for f-s_l (left) and s_i-s_j (middle) are seen more frequent. Note that the r_{ij} fluctuations for c-f (black) and c-s_k (red) in the right column are via the exchange of f and s_k atoms (left column); the central atom does not participate in the permutation because the r_{ij} flips between values 2.5 and 3.8.

low frequency values $\Omega^{(i)}$ at $\omega_L \approx 22$ rad/ps are just such kind of oscillation. The fact that no permutational isomer transition appears for $T \lesssim 150$ K explains why the correlation time is so long. A general feature to observe is that each atom displays a tenacious f-, s-, or c-like behavior. Consequently, the three sets of VAF and their respective power spectra are representative of these three basic behaviors. For temperatures $T > 150$ K, these latter curves are seen to manifest a synthesis of several of these features since the resident time of individual atom in each location becomes shorter with increasing temperature.

(b) Among the 14 atoms, the oscillatory structure of $C^{(f)}$ (green line) shows a short-time ($\sim$0.22 ps) trait which is in opposition to $C^{(s)}$. This short-time characteristic feature persists up to $T=200$ K at which temperature we observed a permutational isomer transition between f and s_i atoms [Fig. 8(a)]. The $C^{(c)}$, on the other hand, is characterized by its distinct rapid oscillation, and it goes on until $T \approx 1250$ K which is defined as T_{melt}.[30] This $C^{(c)}$ property for $T < 1250$ K is unquestionably a manifestation of the solidlike behavior. Referring again to Fig. 6, we found that the c-atom always stays intact at the central location for $T < 600$ K, and it suffers permutations with s_i or f atom at $T=600$ K [Fig. 7(a)] and undergoes more frequent permutations with the s_i atoms only for $T \gtrsim 800$ [Fig. 7(b)]. In the latter circumstances, its oscillatory motion damps out rapidly with increasing temperature. At $T \approx 1250$ K, the oscillatory property in $C^{(c)}$ disappears and the cluster as a whole could have transformed into a liquid since all of 14 $C^{(i)}$ display one similar structure, i.e., a very damped oscillation with only one minimum.

(c) There exists a distinct high frequency peak at $\omega_H \approx 53$ rad/ps in $\Omega^{(c)}$, and the peak persists up to $T \approx 1200$ K. The appearance of this high frequency mode may be understood by recalling a previously calculated VAF of bulk liquid copper[31] which has its first minimum located at about 0.1 ps at $T=1500$ K (Fig. 2 in Ref. 30). This VAF corresponds quite well to the location of the low frequency peak of the power spectrum. Therefore, the high frequency mode in $\Omega^{(c)}$ can be interpreted as the signature of confinement effect arising from the c atom being almost symmetrically surrounded by its neighbors. We should remark that the above VAF of bulk liquid Cu was obtained with a n-body embedded atom model. This n-body potential and the Gupta potential given in Eq. (6) are two widely used interaction potentials for variant applications to bulk systems and clusters. A reference to the bulk VAF and the use of it to infer frequency modes is thus reasonable and instructive. The same kind of nonnegligible high frequency peaks are visible also for s atoms, but due to a lesser number of neighbors and the less symmetrical distribution of surrounding atoms, their existence may be ascribed to a coupling between the c and s atoms. In this case, because the abutting atoms forming the cage have a finite mass and hence do not behave like hard walls, the surrounding atoms thus recoil and this would couple to the c atom. The same argument applies to the high frequency mode of $\Omega^{(f)}$ whose confinement influence is closer to $\Omega^{(s)}$ than $\Omega^{(c)}$ but the coupling is almost imperceptible.

(d) One notices that the departure of the low frequency limits of the power spectra is consistent with the emergence of isomeric permutations. As long as an atom remains at the same location, the corresponding $\Omega^{(i)}$ value is zero. The more it moves from one site to another, the higher will this value increase. As mentioned above, this feature is unambiguously manifested in a bulk metals but is, however, not related to the self-diffusion coefficient in the case of clusters.

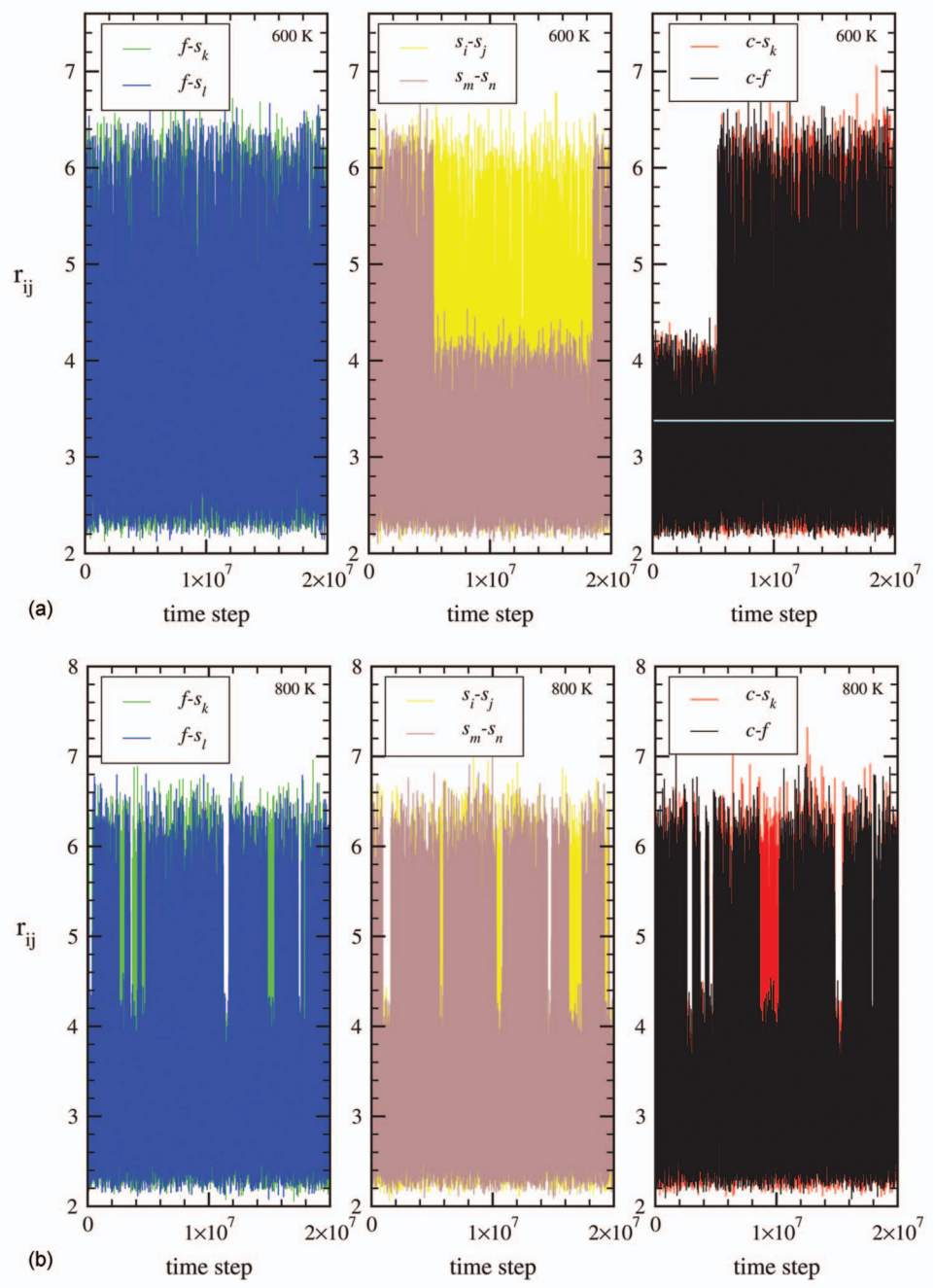

FIG. 7. (Color) (a) Same as Fig. 6 but at $T=600$ K. The figure on the right column shows that the central atom takes part in the permutational isomer transition resulting in the simultaneous up-and-down r_{ij} of c-f (black) and c-s_k (red) for time step greater than $0.5\times10^7\ \Delta t$. (b) Same as Fig. 6 but at $T=800$ K. More frequent permutations are seen among the central, floating, and surface atoms. The frequency of exchange between floating and surface atoms are so high that at this temperature the labels f and s_k may be called "surface" atoms as shown in Fig. 4(c). Together with (a), one may say that an atom spends less and less time at the central location when $T=600\rightarrow800$ K.

B. Bimetallic cluster Ag_1Cu_{13}

1. Specific heat and relative rms bond length fluctuation parameter

The replacement of one Cu atom in Cu_{14} by a Ag atom does not have dramatic consequence on the general characteristic of the specific heat. In fact, the C_V of Ag_1Cu_{13} and Cu_{14} are remarkably similar. For Ag_1Cu_{13}, its C_V continues to show two well-developed peaks one of which is at $T=430$ K which turns out to be the same as the cluster Cu_{14} but is more pronounced and the other at $T\approx1240$ K which is also reasonably close to $T\approx1230$ K of Cu_{14}. The general structure of C_V is therefore strikingly similar. There are, however, distinguishable differences in their δ. For Cu_{14}, Fig. 1 shows that the δ has a two-step structure which is in marked contrast to Ag_1Cu_{13} flaunting a three-step scenario located at $T=170$, 300, and 600 K. Both C_V and δ are displayed in Fig. 9.

As in the case of Cu_{14}, we can understand the mechanism of the three rising steps of δ by appealing to the structures of the lowest energy and different excited states which are delineated in Figs. 10(a)–10(g) and analyzing the energy histograms [Figs. 11(a) and 11(b)] for the probability of emergence of these energy states. The first feature that one notices is that the ground state geometry of Ag_1Cu_{13} is the same as Cu_{14} but the Ag atom becomes the floating atom. This lowest energy structure persists for temperatures $0\leqslant T\leqslant120$ K, whose range is slightly wider than Cu_{14}. Quite different from the cluster Cu_{14}, the fifth excited state appears first at $T=130$ K although its occurrence is extremely low.

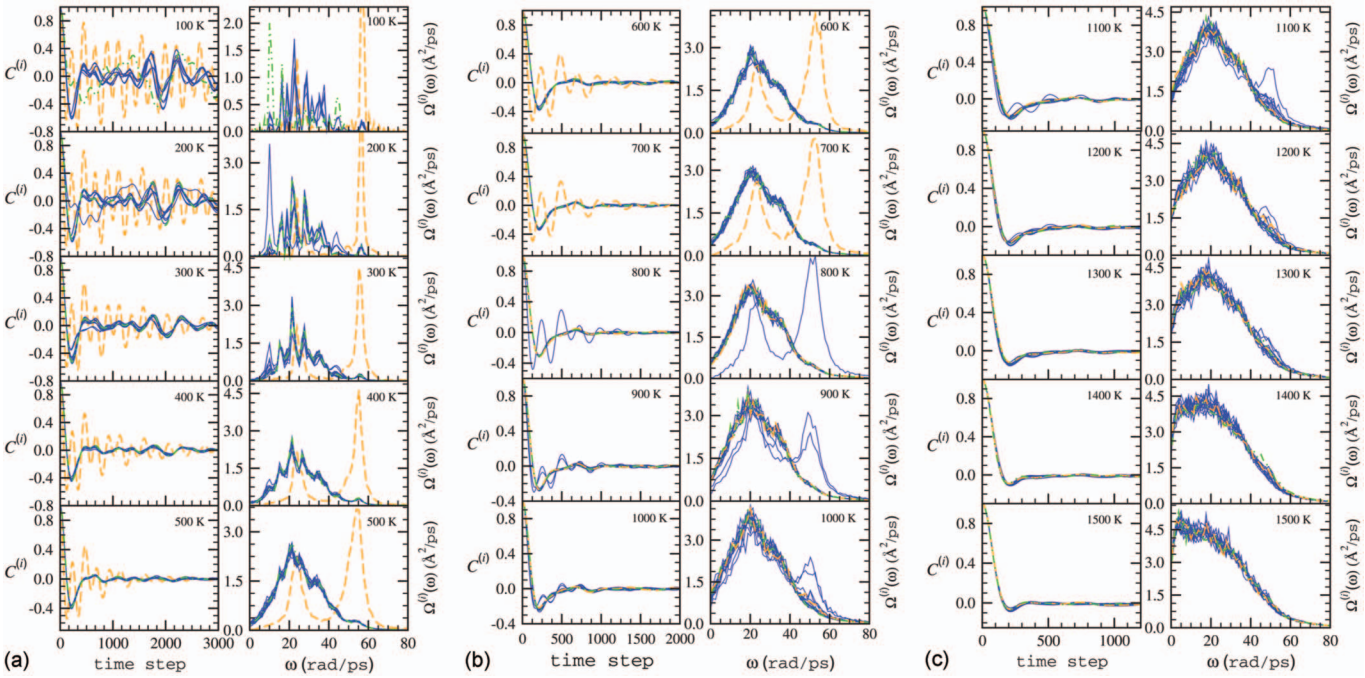

FIG. 8. (Color) Temperature variation of the velocity autocorrelation function (left column) vs time step (in units of 5×10^{-16} s) and power spectrum vs cyclic frequency ω (in units of rad/ps) (right column) for Cu_{14} determined from isothermal Brownian-type MD simulation. The particle is colored orange (dashed line) for center atom, green (dash-dot-dotted line) for floating atom, and blue (solid line) for the rest of surface atoms [consult Fig. 4(c) for the general identification of atoms]. Note that at $T=200$ K, the floating atom has permuted with a surface atom (green→blue), at $T=800$ center and surface (or floating) atoms permute (orange→blue), and at 900 K two surface (or floating) atoms have separately permuted with the center atom.

Then, the first, second, third, fourth, and sixth excited states emerge when the temperature is raised to $T=260$ K. Figure 10 depicts the atomic structure of each of these excited states. Proceeding to a higher temperature $T=300$ K, we observed the seventh, eighth, and ninth excited states and at a still higher temperature $T=360$ K, the tenth. The next higher energy state, the 11th, can be detected only when the temperature has attained $T=800$ K. More and more higher ex-

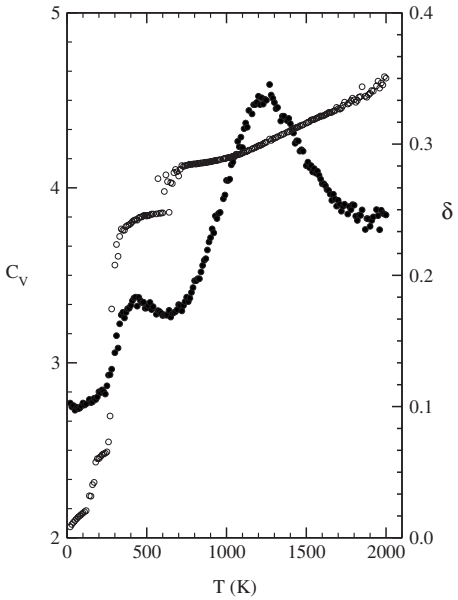

FIG. 9. The constant volume specific heat C_V and relative rms bond length fluctuation constant δ for Ag_1Cu_{13}. The simulation runs were carried out at $\Delta t=10^{-15}$ s.

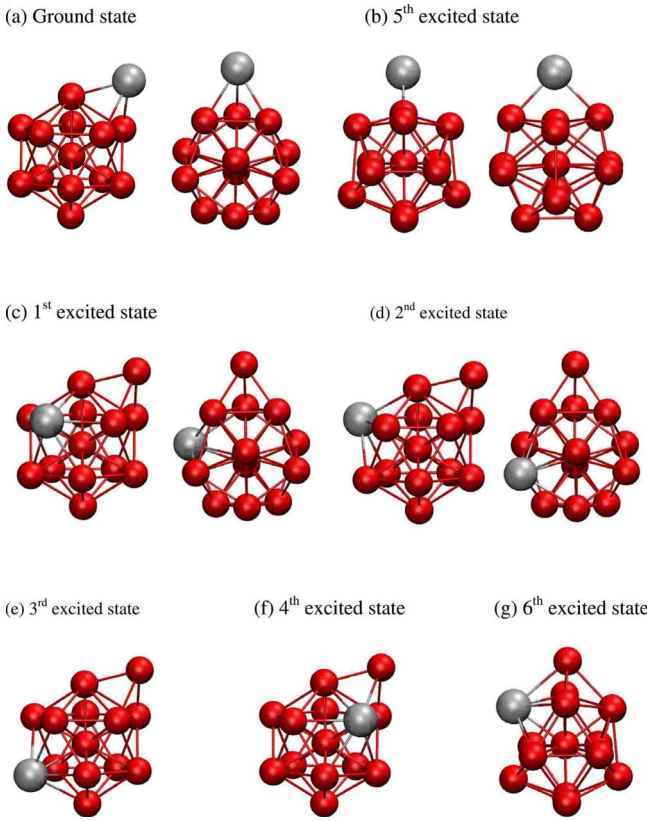

FIG. 10. (Color online) Structures of the lowest energy and excited states for the bimetallic cluster Ag_1Cu_{13}. Note that the fifth excited occurs at a lower temperature. Notation used: Large ball, Ag atom; small ball, Cu atom.

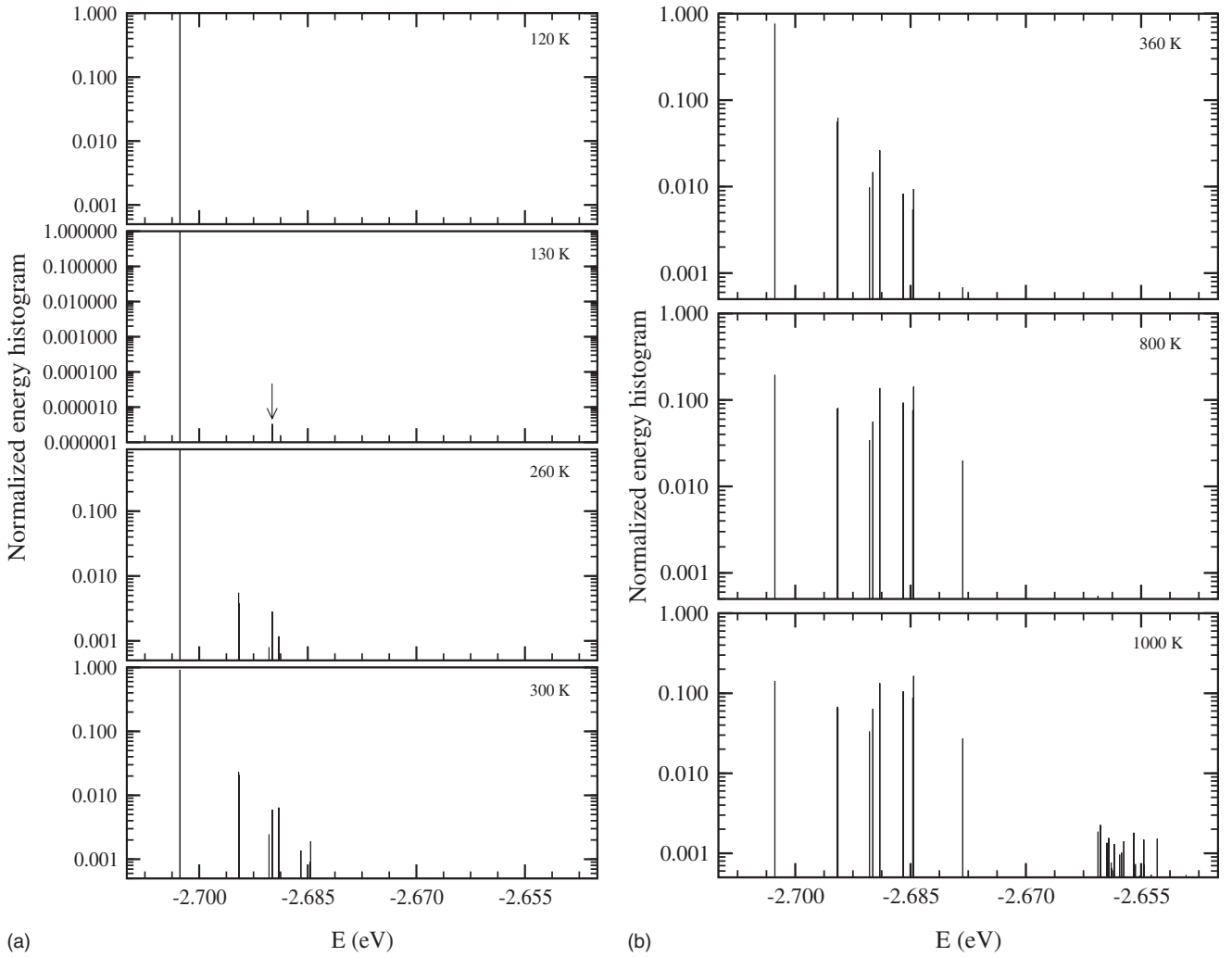

FIG. 11. Energy histograms of Ag_1Cu_{13} constructed from isothermal Brownian-type MD simulations (see text) at temperatures (a) $T=0-120$, 130, 260, 300 K and (b) $T=360$, 800, and 1000 K.

cited states are found for $T \geqslant 1000$ K, which can be gleaned from reading Fig. 11(b). The interested readers are referred to Figs. 11(a) and 11(b) for further details of the probability of occurrence of each of these excited states.

We next turn to an interpretation of the three-step profile of δ. Figures 12(a)–12(o) portray the r_{ij} recorded at different temperatures. These chosen temperatures cover the regimes over which δ climbs up. We summarize four essential features as follows.

(a) For temperatures $0 \leqslant T \lesssim 140$ K, the BC is practically in its lowest energy state and all of 14 atoms behave solidlike. In this temperature range, the fifth excited state occurs [Fig. 11(a)], and it is thus natural to anticipate seeing the r_{ij} fluctuating up and down. This is not so for the r_{ij}'s shown in Fig. 12(a) where they vary horizontally as a function of time. Apparently, the fifth excited state must have survived for a very short time making its ferreting out extremely difficult. At $T=150$ K, the floating atom, which is Ag, merely experiences relocation (blue, f-$s_4 \rightarrow f$-s_3; yellow, f-$s_1 \rightarrow f$-s_2) resulting in the rise and fall of r_{ij}. There is, nevertheless, no permutation among floating, surface, and center atoms (brown, s_1-s_4; black, c-f, green, c-s_1; red, c-s_4). In view of these characteristic features, the first climbing up step of δ may be attributed to the migrational motion of the floating atom Ag. This interpretation may be further confirmed by browsing through Fig. 10 where *only* the fifth excited state has the Ag occupied the floating atom site.

(b) At $T=300$ K, the fluctuations in r_{ij} increase, signaling permutations among the Ag floating atom and surface atoms. At this temperature and for the time period recorded, the center atom Cu *does not* take part in these permutational isomer transitions since the r_{ij}'s (black, green, and red colored lines) remain intact at values approximately 4, 2.4, and 2.4, respectively. We have reached this conclusion mainly based on analyzing concurrently all of r_{ij}'s in Fig. 12(b). As the temperature is increased to $T=500$ K, we found incessant permutations between the f-atom Ag and surface atoms [cf. Figs. 12(c) and 12(e) and also Figs. 12(d) and 12(f)], but the center atom continues to stay untouched at the central position. The second rise in δ can thus be attributed to the resettlement motion of f atom [the rather narrow platforms of Fig. 12(g) (black, c-f)], which is superimposed by the permutational isomer

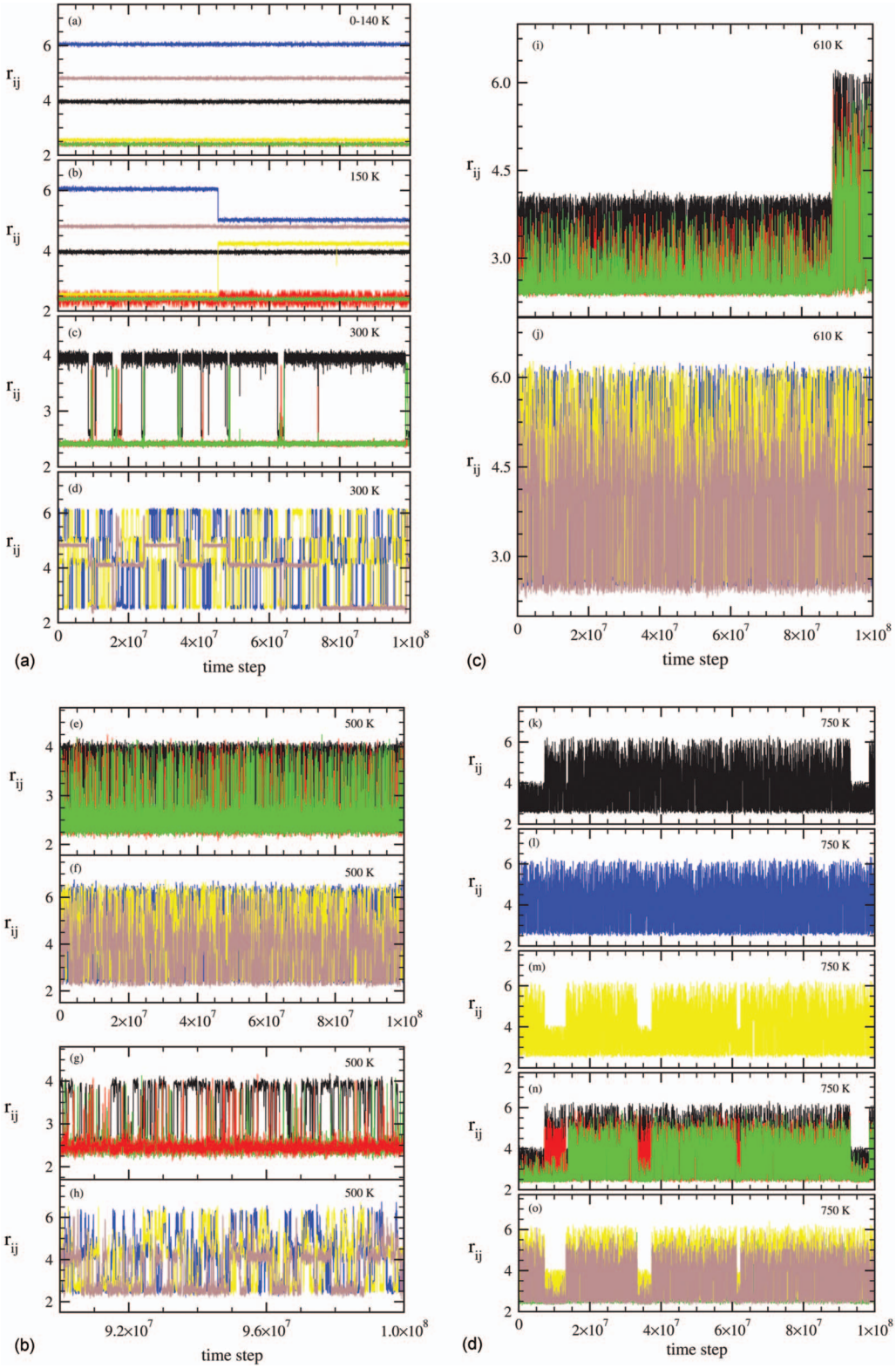

FIG. 12. (Color) (a) Instantaneous relative bond length $r_{ij}(t)$ vs time step (in units of 10^{-15} s) from isothermal Brownian-type MD simulations for Ag_1Cu_{13} calculated at (a) $T=0-140$ K, (b) $T=150$ K, (c) $T=300$ K, (d) $T=300$ K, [(e)–(h)] $T=500$ K, [(i) and (j)] $T=610$ K, and [(k)–(o)] $T=750$ K. The rows (a)–(d) describe $r_{ij}(t)$, with i and j chosen from six sets of two atoms. Refer to Fig. 4(a) for the labeling of f, c, and s_i atoms. Notations used: Yellow, f-s_i; blue, f-s_j; brown, s_i-s_j; green, c-s_i; red, c-s_j; black, c-f. In (b), the up-and-down yellow and blue r_{ij} dictate the migrational relocation of the floating atom. Since s_i-s_j stays constant, there is no permutation between floating and surface atoms. In (c) and (d), which were recorded at $T=300$ K, migrational relocations and permutational isomer transitions for f-s_i (yellow) and f-s_j (blue) have activated fluctuations of s_i in c-s_i (green), s_j in c-s_j (red), and f in c-f (black). The rows (e) and (f) give the instantaneous bond length $r_{ij}(t)$ executing (c-s_i,c-s_j,c-f) and (s_i-s_j,f-s_i,f-s_j) permutations, respectively. The rows (g) and (h) extract from (e) and (f) the parts of time steps running from 9×10^7 to 1×10^8, respectively. It can be seen that at this temperature, permutational isomerizations increase. The center atom, however, does not involve in the permutation. In (i), central atom participates in permutations with floating or surface atom, and in (j) (s_i-s_j,f-s_i,f-s_j) permutations increase rapidly. Finally, in (k)–(o), the permutational isomer transitions from top to bottom are c-f (black), f-s_i (blue), f-s_j (yellow), (c-f,c-s_i,c-s_j) (black, red, green), (s_i-s_j,s_m-s_n,f-s_i) (green, brown, yellow).

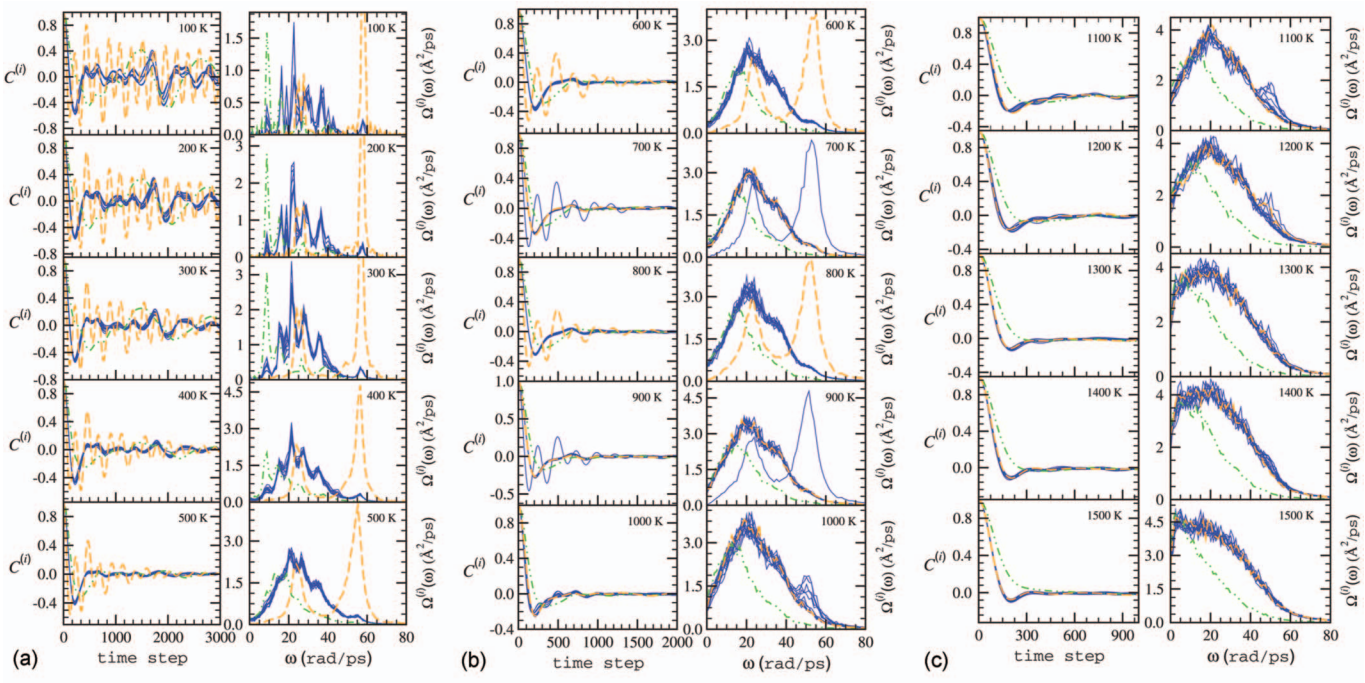

FIG. 13. (Color) Temperature variation of the velocity autocorrelation function vs time step (in units of 5×10^{-16} s^{-1}) (left column) and power spectrum vs cyclic frequency ω (in units of rad/ps) (right column) for Ag_1Cu_{13} determined from isothermal Brownian-type MD simulation. The particle is colored orange (dashed line) for center atom, green (dash-dot-dotted line) for floating atom, and blue (solid line) for the rest of surface atoms [see Fig. 4(c) for the general identification of atoms]. Note that at $T=700$ K, the center atom permutes with a surface atom (orange→blue), and at $T=800$ (blue→orange) and 900 K (orange→blue) center and surface atoms permute.

transition among floating atom and surface atoms (green and red lines, c-s_i).

(c) When the temperature has attained $T=610$ K, the center atom begins its involvement in permuting with floating or surface atoms. Figures 12(i) (green, c-s_i; red, c-s_j; black, c-f or c-s_i) and 12(j) (blue, f-s_i; yellow, f-s_i; brown, s_i-s_j) corroborate these activities. We should emphasize that for $T\geqslant500$ K, the frequency of permutations for the surface-surface or floating-surface atoms are so often that it is, in fact, difficult to tell apart the floating and surface atoms for, at one instant, it is surface atom and, at the next instant, it may be the floating atom. For this reason, we have labeled for the black line c-f or c-s_i permutation. As expected, we observed more and more exchange movements between the center atom and the surface or floating atom when the BC is heated up to $T=750$ K. At this temperature, in the course of permutational isomer transition, all atoms participate in the permutations irrespective of floating, center, and surface. This explains the gear matching of the up-and-down r_{ij} in c-f, f-s_i, c-s_i, and s_i-s_j [Figs. 12(k)–12(o)]. The third ascendant step in δ at $T\approx600$ K can now be comprehended to come from the center atom involving in permutational isomer transition.

(d) At a still higher temperature, we behold an interesting scenario that the Ag atom prefers to stay separated from Cu atoms. This segregating tendency has resulted in the Ag atom comporting an orbital "gaslike" behavior at much higher temperatures (cf. Fig. 13 for the VAF for $T\geqslant1400$ K).

2. Velocity autocorrelation function and power spectrum

We present in Figs. 13(a)–13(c) the change of VAF and spectral densities of Ag_1Cu_{13} with temperature. The general characteristic and the particular traits that merit emphasis are the following two aspects.

(a) The variation of $C^{(i)}(t)$ and of $\Omega^{(i)}(\omega)$ with temperature for the center and surface atoms are very much the same as those of Cu_{14}. For the c atom, $C^{(c)}$ exhibits robust oscillation which may be understood to originate from the thermal oscillation and the oscillation akin to confinement effect. The $C^{(s)}$ of all of the s_i atoms, on the other hand, behave alike; they exhibit vivid oscillatory structures with undiminished correlation times that extend up to 2.5 ps for $T<400$ K. At a higher temperature in the range $400\lesssim T\lesssim500$ K, the extent of undiminished correlation times of $C^{(s)}$ reduce to 1–1.5 ps, and thereafter for $T>500$ K, rapidly transit to one-minimum curves. In the latter circumstance, the correlation times dwindle to magnitudes less than 0.5 ps. For both $\Omega^{(c)}(\omega)$ and $\Omega^{(s)}(\omega)$, a well-resolved low frequency $\omega_L\approx20$ rad/ps may be identified for $T\gtrsim600$ K. This ω_L is reminiscent of the infrared molecular vibration. For $\Omega^{(c)}(\omega)$ in the temperature range $100\lesssim T\lesssim900$ K, there is furthermore a distinct peak at the high frequency $\omega_H\approx56$ rad/ps, which may be interpreted to originate in the cagelike collisions. Considering that the magnitude of $\Omega^{(c)}(\omega_H)$ declines drastically with increasing temperature ($T\gtrsim1000$ K) and

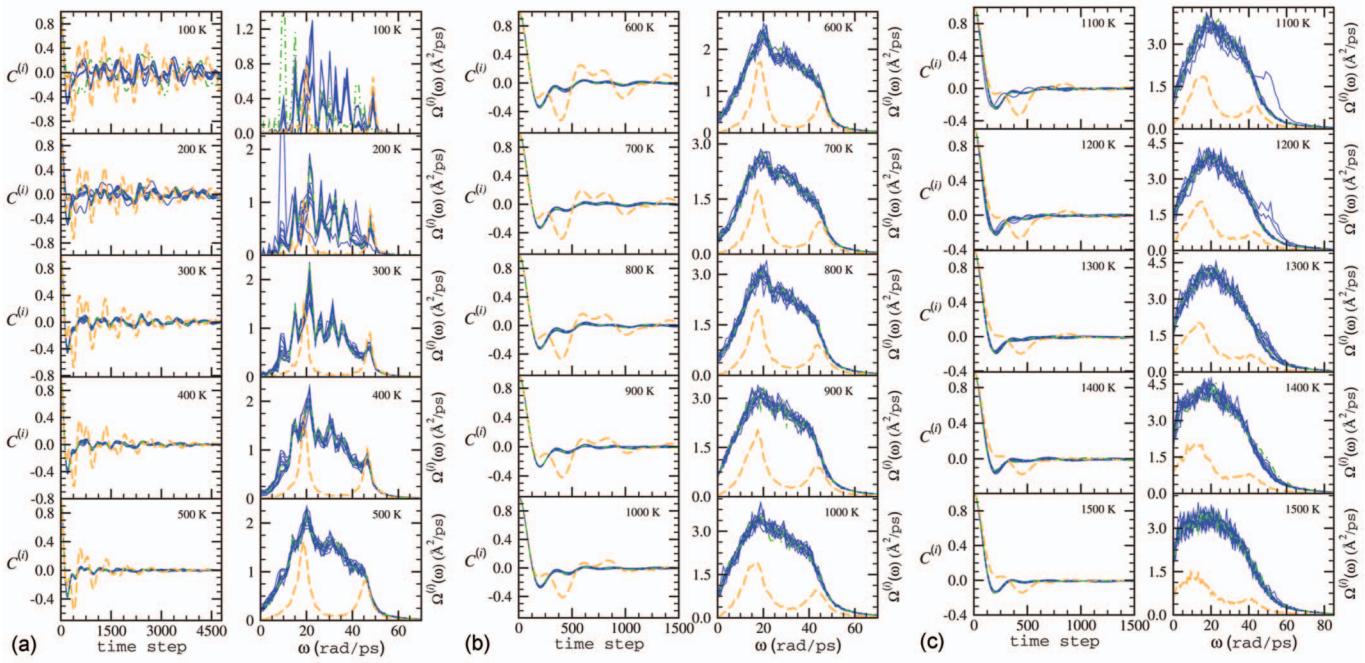

FIG. 14. (Color) Temperature variation of the velocity autocorrelation function vs time step (in units of 5×10^{-16} s) (left column) and power spectrum vs cyclic frequency ω (in units of rad/ps) (right column) for Au_1Cu_{13} determined from isothermal Brownian-type MD simulation. The particle is colored orange (dashed line) for center atom, green (dash-dot-dotted line) for floating atom, and blue (solid line) for the rest of surface atoms [see Fig. 4(c) for the general identification of atoms]. Note that at $T=200$ K, the floating atom permutes with a surface atom (green→blue).

dissolves in $\Omega^{(s)}$ at $T\approx1250$ K [Fig. 13(c)], it is natural to designate the latter temperature (as in the case of Cu_{14}) to be T_{melt}.[30] This temperature is reasonably close to $T_{\text{melt}}\approx1240$ K deduced above from C_V.

(b) For $T\lesssim350$ K, the floating atom Ag behaves solidlike; $C^{(f)}$ oscillates with a correlation time stretching undiminished up to 2.5 ps. At $T\approx400$ K, the extent of the correlation time of $C^{(f)}$ has decreased to approximately 1.63 ps and tapers off with increasing temperature. Accordingly, the temporal characteristic of $C^{(f)}$ as a function of temperature starts with an erratic oscillatory shape for $T\lesssim400$ K, dampens as the surface atoms $C^{(s)}$ at $T=500$ K, but for $T>500$ K, the first minimum of $C^{(f)}$ is seen rounded and shows a proclivity to separate from those of $C^{(s)}$. The interesting feature is the gradual change of the one-minimum structure of $C^{(f)}$ for $500\lesssim T\lesssim1250$ K to a structure characteristic of an orbital gaslike behavior for $T>1250$ K. This thermal behavior of the silver f atom can be gleaned also from the rapid change of $\Omega^{(f)}(\omega)$ at $\omega=0$, and physically it implies the segregating tendency of the Ag atom upon alloying with Cu atoms. In contrast to the $\Omega^{(c)}(\omega)$ and $\Omega^{(s)}(\omega)$, the lower frequency ω_L of $\Omega^{(f)}(\omega)$, which describes the thermal oscillation, has a slightly smaller value.

C. Bimetallic cluster Au_1Cu_{13}

The C_V, r_{ij} (and hence δ), and energy histograms have been reported in a recent article.[8] Here, we direct due attention to the $C^{(i)}(t)$ and $\Omega^{(i)}(\omega)$. Let us start with the lowest energy structure of Au_1Cu_{13}. As illustrated in our previous work, this BC has the same cluster geometry as Cu_{14} and Ag_1Cu_{13} except that the Au atom occupies the central position of the icosahedron. Among the three noble metals, the atomic size of Au is comparable with Ag but is larger than Cu; its mass is, however, the heaviest. Differing from Ag, the Au atom has a mixing tendency on alloying with Cu atoms to form a BC.[32] As a result, its response to temperature is expected to be different from Ag_1Cu_{13} and Cu_{14}, both of which have the Cu atom occupying the central site in icosahedron. We show in Figs. 14(a)–14(c) our simulated $C^{(i)}(t)$ and $\Omega^{(i)}\times(\omega)$. The similarity and incongruity between Au_1Cu_{13} and those of Cu_{14} and Ag_1Cu_{13} can be summarized as follows.

(a) The cause for the incongruity between C_V and δ is the same as the Cu_{14} and Ag_1Cu_{13}. Differing from the latter clusters, there is only a fair agreement in the T_{melt} deduced from C_V, which is $T_{\text{melt}}\approx1393$ K (Fig. 3 of Ref. 8), and that inferred from $C^{(i)}(t)$ or $\Omega^{(i)}(\omega)$, which is $T_{\text{melt}}\approx1250$ K.[30]

(b) For the f atom in Au_1Cu_{13}, which is Cu, we observed the $C^{(f)}(t)$ displaying chaotic oscillation with a clear minimum at approximately 0.25 ps for $T<300$ K. The copper $C^{(f)}(t)$ in this temperature range thus resembles the $C^{(f)}(t)$ of Cu_{14}, where the atom effects the migrational relocation and its motion is interweaved by the permutational isomer transition between f and s_i atoms. These activities tally with the Ag_1Cu_{13}. For $300\leqslant T\leqslant1050$ K, all of 13 copper $C^{(i)}(t)$, $i=s,f$ follow one same pattern, a one-minimum structure, and these structures are further corroborated by the mingling of $\Omega^{(f)}(\omega)$ and $\Omega^{(s)}(\omega)$ into one common spectral density frequency at approximately 20 rad/ps. We should emphasize that the Au atom in this range of temperatures remains intact at the center of the cluster. Thus, al-

though all $C^{(f)}(t)$ and $C^{(s)}(t)$ reveal the typical one-minimum liquidlike structures, the whole cluster has not yet transited to a liquid, for at higher temperatures $T=1100$ and 1200 K there are still some copper atoms [at 1100 K one atom and two at 1200 K, see Fig. 14(c)] permuting with the central atom Au. Nevertheless, for $T \gtrsim 1300$ K,[30] such kind of permutation activities between Cu and Au atoms are so multitudinous that the whole cluster has clearly become a liquid.

(c) Being heavier in mass, the vehement oscillatory frequency of the c atom, in this case the Au atom, has declined (cf. Figs. 8 and 13), and this property of mass has resulted in the shift of high frequency mode to a smaller value at $\omega_H \approx 47$ rad/ps whose $\Omega^{(c)}(\omega_H)$ also assumes a comparatively lower amplitude than $\Omega^{(c)}(\omega_L)$.

IV. CONCLUSION

The isothermal Brownian-type MD simulation has been used to determine the thermal, geometric, and dynamical properties of noble-metal-based BCs. Two BCs, namely, Ag_1Cu_{13} and Au_1Cu_{13}, have been selected for quantitative studies. On the issue of melting temperature, our simulation results reiterated the incongruity that pertains to C_V and δ in estimating a mutually agreed T_{melt}. The discrepancies are ascribed to the permutational isomer transitions among the floating, surface, and central atoms, and for the 14-atom BC also the migrational relocation of f atom. Considering that the lowest energy structure of a 14-atom cluster comprises a 13-atom icosahedron and an adatom sitting outside the icosahedral surface, we confirmed the same cluster morphologies for Cu_{14}, Ag_1Cu_{13}, and Au_1Cu_{13}. There are, however, differences in the atomic distribution. Whereas in Ag_1Cu_{13} the Ag is predicted to occupy the floating atom site, the Au in Au_1Cu_{13}, in contrast, is observed to reside at the central location of the icosahedron. These atomic locations of the impurity atoms in their respective BCs were found to have different bearing on their thermal response. For the Ag atom in Ag_1Cu_{13}, one sees that it has a penchant to segregate from the Cu atoms when it is heated up to a higher temperature ($T \approx T_{\text{melt}}$). Such a disposition can be inferred from scrutinizing the change of $C^{(f)}(t)$ with temperature where the silver $C^{(f)}$ was seen to exhibit first a solidlike structure for $T < 400$ K, become the typical one-minimum liquidlike for $400 \lesssim T < 1300$ K [caused by the f-s_i or c-f permutational isomerization as illustrated by $r_{ij}(t)$ in Figs. 12(e)–12(o)], and switch to comport itself as an orbital gaslike for $T \gtrsim 1300$ K. On the other hand, for the Au atom in Au_1Cu_{13}, we beheld that it prefers to be surrounded by other (surface and floating) Cu atoms. This aptitude for different kind of neighbors is manifested by the temperature dependences of $C^{(c)}$ revealing robust solidlike oscillation for $T < 1100$ K and continuing to deport itself liquidlike for $T \gtrsim 1100$ K. The Au atom in Au_1Cu_{13} is undoubtedly exhibiting a mixing tendency. Again, mutual consistency in the variations of $C^{(c)} \times(t)$ and $r_{ij}(t)$ (Figs. 6 and 10 of Ref. 8) with temperature divulges just such kind of microscopic dynamics for the Au atom. With more in-depth analysis on $C^{(i)}(t)$ and $\Omega^{(i)}(\omega)$ supplemented further by the cluster structures, energy histograms, and instantaneous relative bond length, the T_{melt} of a cluster can be reasonably estimated. For the noble-metal-based clusters considered in this work, we have, in fact, found T_{melt} deduced from $C^{(i)}$ and $\Omega^{(i)}$ to be in accord with that inferred from C_V.

ACKNOWLEDGMENTS

This work is supported (NSC96-2112-M-008-018-MY3) by the National Science Council, Taiwan.

[1] G. E. Lopez and D. L. Freeman, J. Chem. Phys. **98**, 1428 (1993).
[2] M. J. López, P. A. Marcos, and J. A. Alonso, J. Chem. Phys. **104**, 1056 (1996).
[3] E. B. Krissinel and J. Jellinek, Chem. Phys. Lett. **272**, 301 (1997); Int. J. Quantum Chem. **62**, 185 (1997).
[4] S. P. Huang and P. B. Balbuena, J. Phys. Chem. B **106**, 7225 (2002).
[5] S. K. R. S. Sankaranarayanan, V. R. Bhethanabotla, and B. Joseph, Phys. Rev. B **71**, 195415 (2005).
[6] A. Aguado and J. M. López, Phys. Rev. B **72**, 205420 (2005).
[7] K. Michaelian and I. L. Garzón, Eur. Phys. J. D **34**, 183 (2005).
[8] T.-W. Yen, S. K. Lai, N. Jakse, and J. L. Bretonnet, Phys. Rev. B **75**, 165420 (2007).
[9] J. Jellinek, T. L. Beck, and R. S. Berry, J. Chem. Phys. **84**, 2783 (1986).
[10] T. L. Beck, J. Jellinek, and R. S. Berry, J. Chem. Phys. **87**, 545 (1987).
[11] T. L. Beck and R. S. Berry, J. Chem. Phys. **88**, 3910 (1988).
[12] I. P. Buffey, W. B. Brown, and H. A. Gebbie, J. Chem. Soc., Faraday Trans. **86**, 2357 (1990).
[13] F. S. Zhang, E. Suraud, F. Calvo, and F. Spiegelmann, Chem. Phys. Lett. **300**, 595 (1999).
[14] V. de Coulon, P. Delaly, P. Ballone, J. Buttet, and F. Reuse, Z. Phys. D: At., Mol. Clusters **19**, 173 (1991).
[15] P. Delaly, P. Ballone, and J. Buttet, Phys. Rev. B **45**, 3838 (1992).
[16] J. Jellinek and A. Goldberg, J. Chem. Phys. **113**, 2570 (2000).
[17] Z. B. Güvenc, J. Jellinek, and A. F. Voter, in *Physics and Chemistry of Finite Systems: From Clusters to Crystals*, edited by P. Jena, S. N. Khanna, and B. K. Rao (Kluwer, Dordrecht, 1992), Vol. 1, p. 411.
[18] M. H. Güven and M. Eryürek, Phys. Status Solidi B **213**, 283 (1999).
[19] H. Arslan and M. H. Güven, New J. Phys. **7**, 60 (2005).
[20] C. Borgs and R. Kotecky, J. Stat. Phys. **79**, 43 (1995).
[21] S. Nosé, J. Chem. Phys. **81**, 511 (1984); Mol. Phys. **52**, 255 (1984).
[22] D. Kusnezov, A. Bulgac, and W. Bauer, Ann. Phys. (N.Y.) **204**, 155 (1990); A. Bulgac and D. Kusnezov, Phys. Rev. A **42**, 5045 (1990).
[23] F. Cleri and V. Rosato, Phys. Rev. B **48**, 22 (1993).
[24] C. H. Chien, E. Blaisten-Barojas, and M. R. Pederson, J. Chem. Phys. **112**, 2301 (2000).
[25] C. Mottet, G. Tréglia, and B. Legrand, Phys. Rev. B **46**, 16018 (1992).
[26] D. Liu and J. Nocedal, Math. Program. Ser. B **45**, 503 (1989).
[27] J. E. Adams and R. M. Stratt, J. Chem. Phys. **93**, 1332 (1990).
[28] J. F. Wax, R. Albaki, and J. L. Bretonnet, Phys. Rev. B **65**, 014301 (2002).
[29] D. A. McQuarrie, *Statistical Mechanics* (Harper and Row, New York, 1976).
[30] Here, the mergence of *all* of 14 $\Omega^{(i)}$ and the simultaneous disappearance of $\Omega^{(c)}(\omega_H)$ is defined to be T_{melt}.
[31] F. F. Chen, H. F. Zhang, F. X. Qin, and Z. Q. Hu, J. Chem. Phys. **120**, 1826 (2004).
[32] P. J. Hsu and S. K. Lai, J. Chem. Phys. **124**, 044711 (2006).